



Research Article

Investigation of the Wear Behavior of AA6063/Zirconium Oxide Nanocomposites Using Hybrid Machine Learning Algorithms

R. Reena Roy,¹ Leninisha Shanmugam,¹ A. Vinothini,¹ Nirmala Venkatachalam ,² G. Sumathy,³ Bhavadharini Murugesan,¹ P. Mercy Rajaselvi Beaulah,¹ and Gizachew Assefa Kerga ⁴

¹School of Computer Science and Engineering, Vellore Institute of Technology, Chennai, Tamilnadu, India

²Department of Artificial Intelligence and Data Science, Easwari Engineering College, Chennai, Tamilnadu, India

³Department of Computational Intelligence, Faculty of Engineering and Technology, SRM Institute of Science and Technology, Kattankulathur, Chennai, Tamilnadu, India

⁴Department of Chemical Engineering, College of Biological and Chemical Engineering, Addis Ababa Science and Technology University, Addis Ababa, Ethiopia

Correspondence should be addressed to Gizachew Assefa Kerga; gizachew.assefa@aastu.edu.et

Received 5 November 2022; Revised 24 March 2023; Accepted 26 April 2023; Published 18 May 2023

Academic Editor: B. R. Ramesh Babu

Copyright © 2023 R. Reena Roy et al. This is an open access article distributed under the Creative Commons Attribution License, which permits unrestricted use, distribution, and reproduction in any medium, provided the original work is properly cited.

This research created hot-pressed composites of the AA6063 matrix with varying concentrations of ZrO₂ (0.25, 0.5, and 1 wt %). At sliding speeds of 80, 120, and 150 mm/s, the wear performance of the specimen was studied at loads of 10 N, 15 N, 20 N, and 25 N. The authors analyzed the counter-face material, the wear debris, and the worn surfaces to learn about the wear mechanisms. Developing these three machine learning (ML) algorithms was to evaluate the ability to predict wear behavior using the same small dataset collected using varying test processes. A thorough examination of each model hyperparameter tuning phase was performed. The predictive performance was analyzed using several statistical tools. The most effective decision-making algorithms for this data collection were those based on trees. Predictions made by the decision tree algorithm for the test and validation measurements have an accuracy of 86% and 99.7%, respectively. The best model was picked out based on the results of the predictions.

1. Introduction

Aluminum (Al) has considerable potential to be utilized in the aviation and automation industries to minimize emissions owing to its less density, well machinability, damping capability, and recyclability. Al has a less elastic modulus, minimal wear resistance, and a maximum corrosion rate, which are all significant problems. Various particle reinforcements have been reported to be added to the Al alloy matrix to solve these issues [1].

Unfortunately, weak tribological characteristics are a drawback of Al alloys. Compared to pure Al alloys, AMMCs (aluminum metal matrix composites) perform better in strength, stiffness, and wear [2]. AMMCs incorporate Al alloys with various reinforcements, including

SiC, Al₂O₃, B₄C, TiB₂, CNT, and GNPs [3]. Due to its outstanding thermal stability, Al₂O₃ is widely used in many applications. As a result, the metal matrix and the reinforcement elements do not go through the brittle phase. So, because of its exceptional characteristics, Al₂O₃ is frequently used in the manufacturing of AMMCs [4].

Aerospace applications for the high-strength AA6063 include fasteners, shafts, and gears. The natural deterioration of these parts through rubbing is important [5]. Therefore, significant breakdowns in industrial operations may result from material loss due to wearing [6]. For this reason, investigating how AMMCs behave tribologically is essential. It is common knowledge that running trials to determine wear behavior is time consuming and costly. Machine learning strategies are used to cut down on the cost and duration of

probes. By analyzing past wear patterns, these techniques allow for accurate predictions of future behavior [7]. The surface roughness and wear loss of materials are predicted using a variety of machine learning techniques, including artificial neural networks (ANNs) [8], support vector regression (SVR), and extreme learning machines (ELMs) [9]. In addition, the effect of several wear factors (sliding speed, load, and sliding distance) was investigated using analysis of variance (ANOVA).

Most industrial procedures can be classified as either solid-state or liquid-state processes. The mechanical properties of solid-state processes are far superior to those of their liquid-state counterparts. Improved mechanical properties are linked to decreased segregation and intermetallic phase formation [10].

Machine learning (ML) was the only available method to solve the computational problems of big data science. Glasses and alloys have intricate and disordered microstructures and have benefitted from ML approaches in comprehending composition-engineering property relationships [11]. Mechanical property predictions can also be made with reasonable accuracy using ML methods based on atomistic descriptors. For instance, an ANN can be trained to estimate organic structure composites based on structural or topological properties [12].

Pumps, bearings, propellers, engineering tools, and dies all benefit from copper alloys' excellent strength, hardness, wear resistance, and abrasive resistance [13]. The material's high tensile strength and hardness exemplify the mechanical properties of aluminum bronze. Right now, we must resort to destructive testing methods that are both expensive and time consuming to evaluate the mechanical parts made of aluminum bronze. Therefore, there is an immediate need for a reliable means of evaluating aluminum bronze's mechanical qualities.

Predicting the mechanical properties of materials using machine learning techniques has grown increasingly popular in recent years. The author found that the back-propagation artificial neural network (BP-ANN) model could reliably forecast AMC's bending toughness and hardness [14]. The strength of aluminum-copper-magnesium-silver alloys was predicted using support vector regression (SVR) [15]. This research showed that, compared to BP-ANN, SVR models performed better under controlled conditions. The author developed a high-precision ANN model to forecast the UTS of niobium-silicon alloy [16]. The model was essential in facilitating their mission of improving specimen strength by modifying its microstructure. The authors [17] employed an ANN model to predict the mechanical properties of A357 alloy, and their results show that the back-propagation model is very accurate. Using an artificial neural network model, the authors [18] could predict the HB of 18-5PH and fine-tune a temperature treatment protocol to achieve maximum HB.

Since its inception over 20 years ago, the field of artificial intelligence, known as machine learning, has been an indispensable and foundational part of many businesses. Although ML was initially researched in the field of computer science and mathematics, it is often preferred

by researchers to use low-content nano-reinforcement particles rather than high-range microsupsplements [19]. Nano-reinforcements improve particular strength and flexibility without compromising density, in contrast to microreinforcements.

Only a few investigations on Al/ZrO₂ composites were found when searching the academic literature. The authors investigated the corrosion and mechanical performance of powder metallurgy-produced nanocomposite Al-0.5 Zn/1.0 ZrO₂ [20]. Composite materials, they said, have greater compressive strength than pure aluminum. Al/1 ZrO₂ composite has also been reported to have the highest corrosion resistance [21]. Disintegrated melt deposition of Al yields mechanical and flammability qualities, which were studied by the authors [22], who looked at the impact of ZrO₂ particle size (submicron, micron, and nano) on these characteristics.

The exceptional success of machine learning in forecasting the outcomes of expensive and time-consuming trials makes it a crucial tool for predicting the wear performance of Al matrix composites [23]. No research was found in the literature studies that indicated the wear behavior of AA6063/ZrO₂ composites.

This research examines the various machine learning models (support vector regressor, random forest, and decision tree) that can forecast how the AA6063/ZrO₂ composites will perform under wear conditions. Powder metallurgy was used to create 0.25 wt%, 0.5 wt%, and 1 wt% AA6063/ZrO₂ composites. Sliding at 80 mm/s, 120 mm/s, and 150 mm/s while applying 10 N, 15 N, 20 N, and 25 N was used to assess the wear performance samples. It was determined that three-machine learning algorithms could be used to forecast the wear performance of the sample.

2. Experimental Density

The matrix and reinforcing materials are AA6063 and ZrO₂ powders, respectively. The matrix material has an even distribution of the elements Zn (0.1 wt %), Cu (0.1 wt %), Si (0.6 wt %), and Al (0.1 wt %) in its chemical composition. The average particle size of AA6063 powder is 40 μm, while 99.35% ZrO₂ comes in at 78 nm. Methanol is used as an etching solution to clean the specimen before SEM analysis. Powdered AA6063 and ZrO₂ are depicted in Figures 1(a) and 1(b) using scanning electron microscopy (Carl Zeiss MA15/EVO 18).

The composites were made with ZrO₂ in three distinct weight percent fractions: 0.25%, 0.5%, and 1%. ZrO₂ nanoparticles were found to have a vol% of 0.25%, 0.5%, and 1%. It took 12.5 grams of powder per output unit to achieve this blend. After subjecting the ZrO₂ nanopowders to ultrasonic vibration treatment, the AA6063 matrix powders were added. The composites were blended at a temperature of 190°C using a void distillation technique. Due to its low boiling point of 78.3°C, alcohol quickly evaporated from the mixture. Once the powder was well mixed, it was put into the graphite mold. A hot-pressing furnace with a controlled environment was used in the manufacturing process. The time spent hot pressing was 1 hour, the temperature was

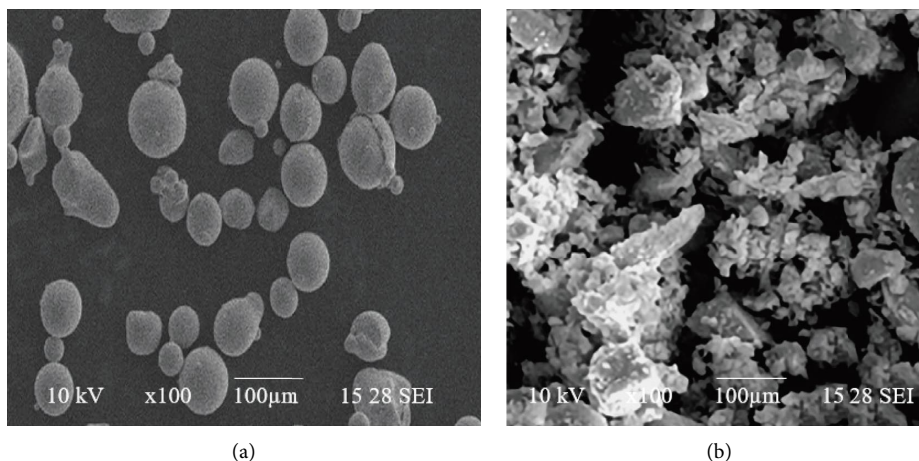


FIGURE 1: Scanning electron microscope of (a) AA6063 and (b) ZrO_2 powders.

525°C, and the pressure was 45 MPa. Creating everything was carried out in an argon-filled environment.

The manufactured composite specimen has a radius of about 16 mm and an altitude of about 8 mm. Tests for measuring hardness were conducted using Vickers hardness test equipment (FIE, VM50) with a 1 kg load. The authors took seven readings from each sample and calculated the hardness based on the mean value.

When calculating density, a 0.1 mg resolution Kern electronic balance was used. Archimedes' principle was used to calculate the actual and relative densities of the specimen. Both air and distilled water were used to make accurate weight measurements of the samples. The applicable formula used in the calculation is as follows:

$$\rho = \frac{m_a}{m_a - m_w} \rho_w, \quad (1)$$

where ρ is the density of the sample (g/cm^3), m_a is the mass of sample in the air, m_w is the mass of the sample in water, and ρ_w is the density of the water.

X-ray diffraction (XRD) was used to identify the phases generated during the manufacturing of AA6063 matrix composites. The microstructure was inspected using scanning electron microscopy (SEM) coupled with an energy dispersive spectrometer (EDS).

Under dry sliding conditions, the wear behavior of Al/ ZrO_2 nanocomposites was investigated using a reciprocating tribometer device. Ten, fifteen, twenty, and twenty-five-newton loads at speeds of 80, 120, and 150 mm/s are used in wear tests. One hundred meters was the slide distance. The authors used AISI 420 stainless steel balls for the countertops. The wear cross-section of the specimen was calculated precisely after the abrasion tests were completed. Multiplying the cross-sectional area by the stroke distance yields the lost volume (ml).

3. Results and Discussion

3.1. Density and Microstructural Properties. Table 1 displays the outcome of density testing on AA6063 and AA6063/ ZrO_2 composites. The theoretical and actual densities of the

samples show a remarkable degree of agreement. This demonstrates that AA6063/ ZrO_2 composites may be produced using hot pressing. To achieve the highest relative density, the AA6063 alloy was used. Increasing the percentage of ZrO_2 in the samples causes them to become less dense in comparison [24]. A high melting temperature of ceramic nanoparticles hinders compressibility and impairs consolidation, leading to a lower relative density and hence greater porosity [25]. The authors [26] found that as the ZrO_2 content of the composites with an Al matrix increased, the porosity of the composites also increased. The reports show less than 1.5% overall porosity [27]. The density findings of this investigation are found to be compatible with the literature.

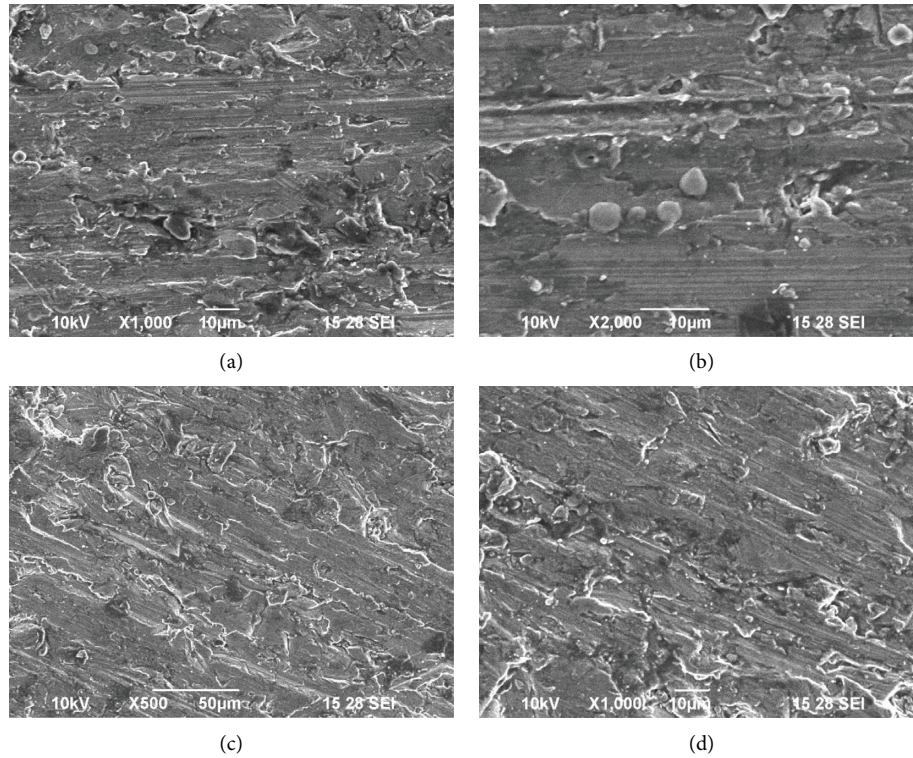
SEM micrographs with magnification of 500X, 1000X, and 2000X of the samples, displayed in Figures 2(a)–2(d), reveal that neither defects nor microporosity are present. The intermetallic phase and the nanoparticles are shown to be in motion. It is easy to see the intermetallic stages in Figure 2(a). The authors [28] reported that AA6063 alloys could generate Al-Zr intermetallics. ZrO_2 nanoparticle aggregation is observed for all composite materials irrespective of ZrO_2 concentration. The increased surface area of nanoparticles is evidence of their accumulation in the composite structure [29]. Nanoparticle aggregation was reported for AA6063/2 ZrO_2 composite.

The EDS results for the AA6063 alloy are shown in Figure 3. A high concentration of Al and a relatively low Zr content were found in the first analytical zone. It is good to know that the AA6063 alloy's chemical arrangement has been confirmed [30]. The high concentrations of Al and Zr found in the white particles (area 2) study identify them as Al-Zr intermetallic complexes. High O content in the structure also allows for the production of Al_2O_3 . In the literature [31], Al matrix composites with Al_2O_3 were mentioned. Oxide production is linked to increased chemical action among Al and O.

These graphs display Al, O, and Zr abundance within the mapped region. The analysis conclusively demonstrated that Al makes up a large percentage of the area. High O

TABLE 1: Specimen's density.

Specimens Units	Theoretical density (g/cm ³)	Experimental density (g/cm ³)	Relative density (%)
AA6063 alloy	2.70	2.68	99.25
AA6063/0.25 ZrO ₂	2.71	2.69	99.26
AA6063/0.5 ZrO ₂	2.72	2.70	99.26
AA6063/1 ZrO ₂	2.73	2.72	98.63

FIGURE 2: SEM photograph of the specimens: (a) AA6063, (b) AA6063/0.25 ZrO₂, (c) AA6063/0.5 ZrO₂, and (d) AA6063/1 ZrO₂.

distribution is also observed near grain borders. Zr was also found to be present in some locations.

The XRD patterns of AA6063, AA6063/0.25 ZrO₂, AA6063/0.5 ZrO₂, and AA6063/ZrO₂ composites are presented in Figures 4(a)–4(d). The analysis confirmed the Al phase present in the samples. The peak of the Al-Zr phase can also be seen for unreinforced alloy and composite materials [32]. Evidence of Al-Zr intermetallic compounds was verified by EDS and XRD investigation. For composites, there was no ZrO₂ peak observed. As a result of the minimal ZrO₂ in the composites, ZrO₂ peaks cannot be kept in complete constant perusing [33]. X-ray diffraction (XRD) examination of an Al/2 ZrO₂ composite was claimed to show no ZrO₂ peaks authors [24]. The test was held at a constant of between 2 and the square root of 2 or between 28.5 and 30.5. It was possible to determine both the step size (0.05) and the counting period (60 s). The inset of Figure 5 provides the value of 2 equal to 29.6, at which the ZrO₂ peak was observed.

3.2. Wear Test and Hardness Results. Table 2 displays the range of the hardness produced in the specimen. The results show that as the ZrO₂ level of the samples rises, hardness

increases. This study found that the AA6063/1 ZrO₂ sample had the highest hardness (83 HV). Hardness increased from 6.2% for AA6063/0.25 ZrO₂ to 9.5% for AA6063/0.5 ZrO₂ and 14.5% for AA6063/1 ZrO₂. ZrO₂ nanoparticle indentation resistance is linked to hardness improvement in composite materials. In addition to preventing dislocation movement, the reinforcing particles are responsible for the hardness increase.

A plot of volume loss versus load for variant sliding speeds is indicated in Figure 6. It is clear from the plots that for every sliding speed and load, volume loss declines with rising ZrO₂ content. In terms of volume loss, the AA6063/1 ZrO₂ sample showed the highest durability over time. Furthermore, with a load of 25 N and a sliding speed of 80 mm/s, for instance, the volume loss of the AA6063 was recorded to be 1.56 (mm³), but it fell to 1.13 (mm³) for the AA6063/1 ZrO₂. The volume loss of AA6063/1 ZrO₂ was 18.6% less than that of unreinforced AA6063 when sliding at 150 mm/s while under a stress of 25 N. Increased wear behavior for MMC materials has been attributed to several distinct causes in the published literature. One of the crucial wear-increasing mechanisms [34] involves the resistance of

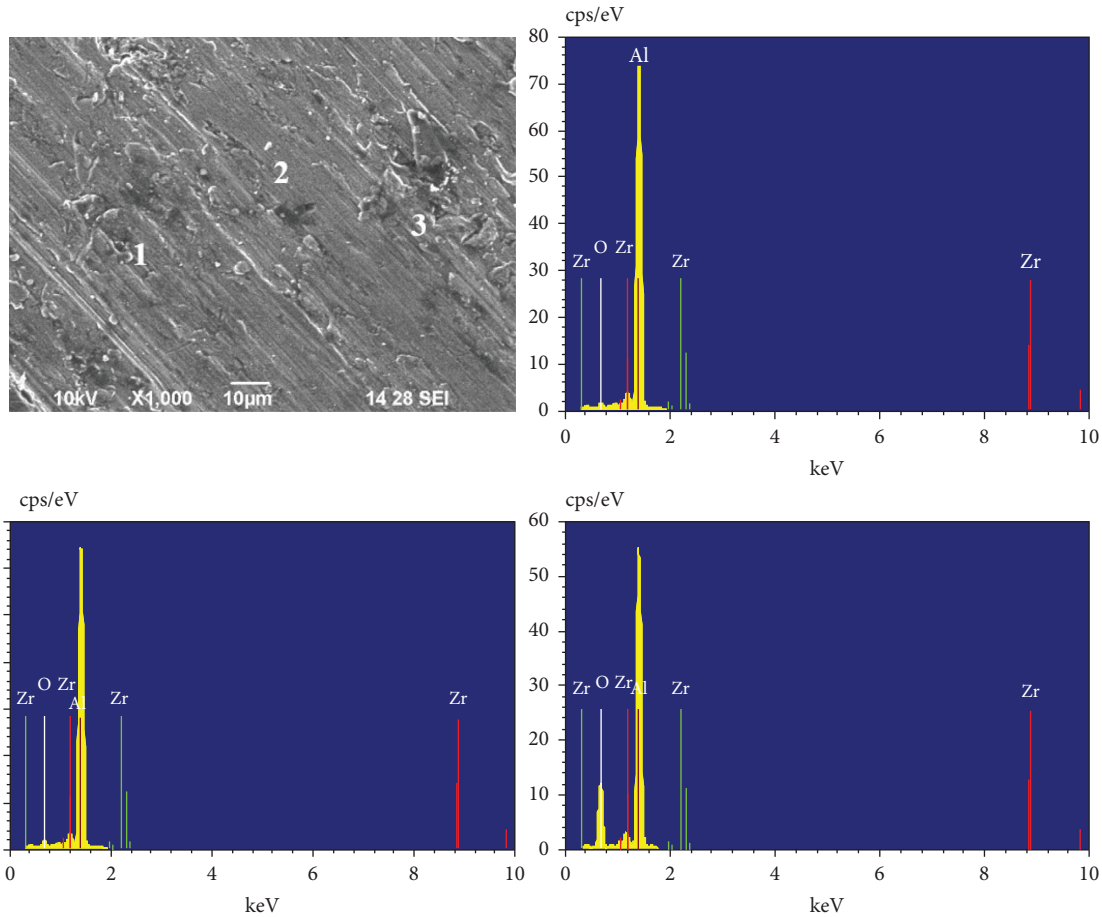
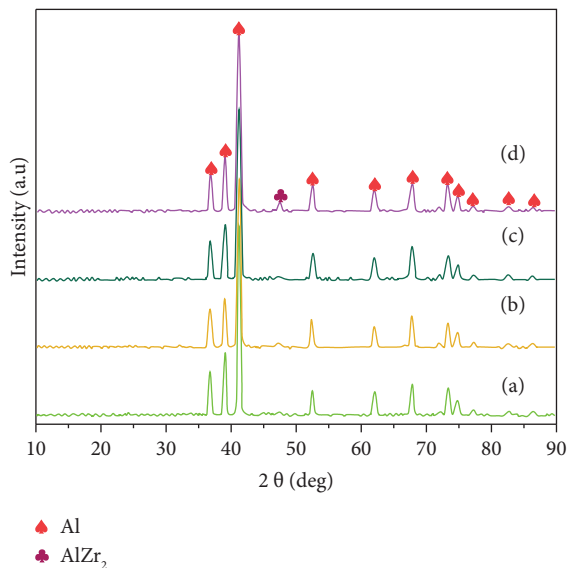


FIGURE 3: AA6063 analysis by EDS.

FIGURE 4: X-ray diffraction of (a) AA6063, (b) AA6063/0.25 ZrO₂, (c) AA6063/0.5 ZrO₂, and (d) AA6063/1 ZrO₂.

high-hardness reinforcement elements in the composite material's structure to wear degradation. The particles of reinforcement are said to bear the weight of the structure [35].

Reducing the surface area of contact between the MMC and the steel counterpart is crucial for better tribological behavior. In Figure 6, it is evident that an increase in the applied load results in a noticeable rise in the wear rate for both samples, as measured by volume loss. The wear rate of Al/ZrO₂ nanocomposites (0.3 and 0.6 wt%) increases with rising loads (from 5 N to 30 N), as observed by a researcher [36].

A plot of volume loss vs. sliding speeds for various loads is shown in Figures 5(a)–5(d). The authors saw that increasing the sliding speed reduces the volume loss across the board for all materials for a given weight. For instance, it was measured that the volume loss of AA6063/ZrO₂ under a load of 25 N varied from 1.13 (mm³) for a sliding speed of 80 mm/s to 0.91 (mm³) for a speed of 120 mm/s and 0.78 (mm³) for a speed of 150 mm/s. The volume loss rises in the limits of 80 to 120 mm/s, then falls in the range of 110 mm/s and above (except for AA6063 under the load of 15 N). Surface hardness enhances wear behavior by decreasing contact area, and strain rate and surface hardness increase with increased sliding speed [37].

The authors found the wear rate of the Al/BN nanocomposite to lessen as the sliding speed was increased (from 80 to 180 mm/s) [38]. Researchers [39] analyzed a varied wear behavior for the Al alloy under minimal load and variable sliding speed, in contrast to the literature above

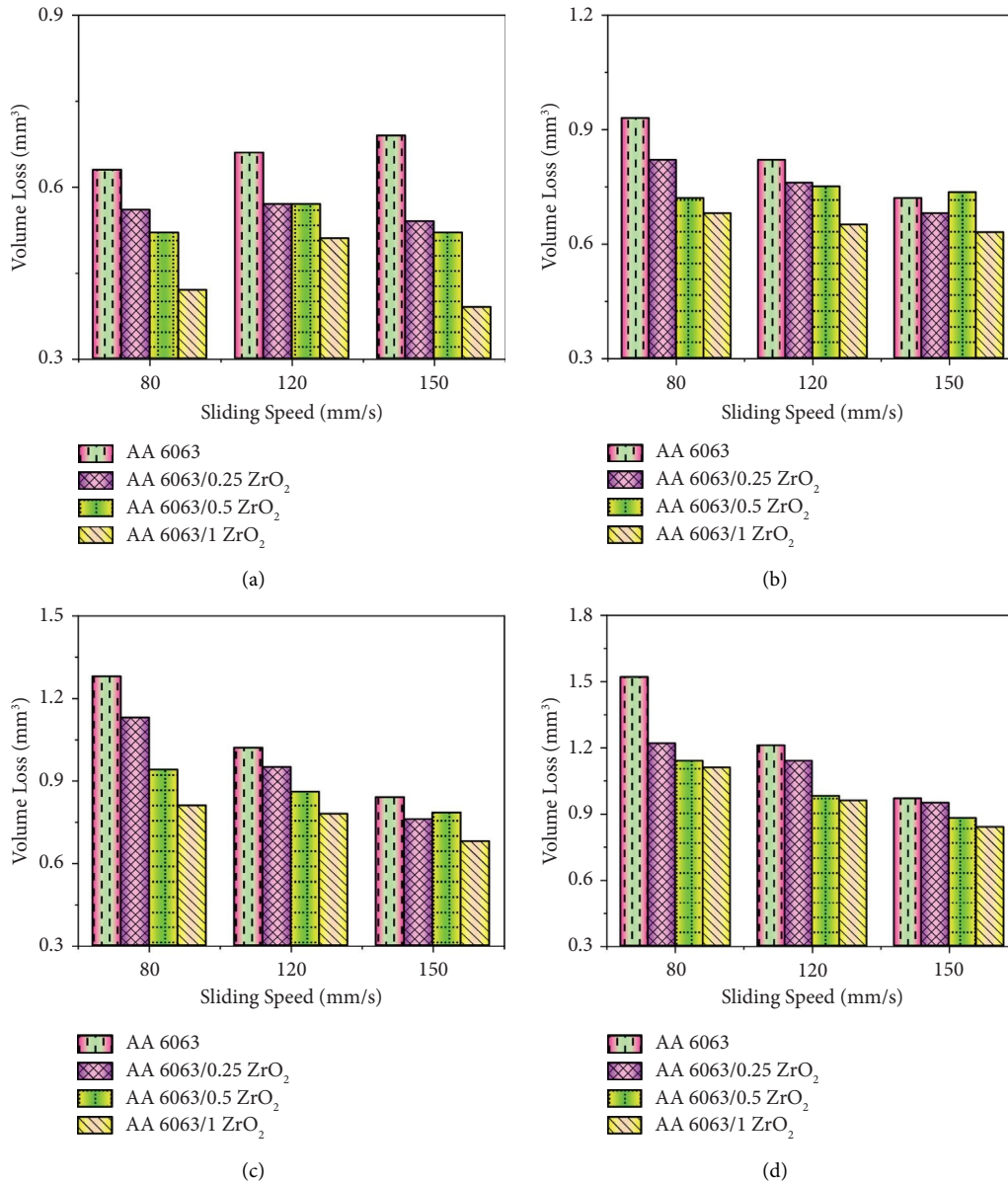


FIGURE 5: Variation of volume loss and sliding speed at variant loads: (a) 10, (b) 15, (c) 20, and (d) 25 N.

TABLE 2: Specimen's hardness.

Materials	Hardness (HV1)
AA6063	83.2 ± 1.3
AA6063/0.25 ZrO ₂	84.7 ± 1.7
AA6063/0.5 ZrO ₂	89.6 ± 1.8
AA6063/1 ZrO ₂	91.9 ± 2.1

investigations. A higher wear rate was seen up to a sliding speed of 0.1 mm/s, after which it was observed to decrease. The authors concluded that this was because the frictional heat produced among the matrix and the counter material significantly impacted the wear process. The contact temperature and surface oxidation both rise as sliding velocity

increases. Because the surface is being oxidized, friction and wear are reduced. The outcome of the low-load wear test for this investigation agrees with the study's findings [40].

In addition, Figure 5 shows wear behavior as a function of the ZrO₂ level. The volume loss diminishes with rising ZrO₂ for all weights and sliding speeds. Compared to AA6063 alloy, the volume loss of the AA6063/1 ZrO₂ composite was 44.6% less under a load of 10 N and a sliding speed of 80 mm/s. The volume loss of an AA6063 alloy decreased from 1.44 (mm³) to 1.01 (mm³) when loaded with 25 N while sliding at 80 mm/s, with the addition of 1 wt % ZrO₂. ZrO₂ nanoparticle incorporation significantly increased wear resistance under both low and high loads. Incorporating nano-sized ZrO₂ particles into composites results in a material with a much

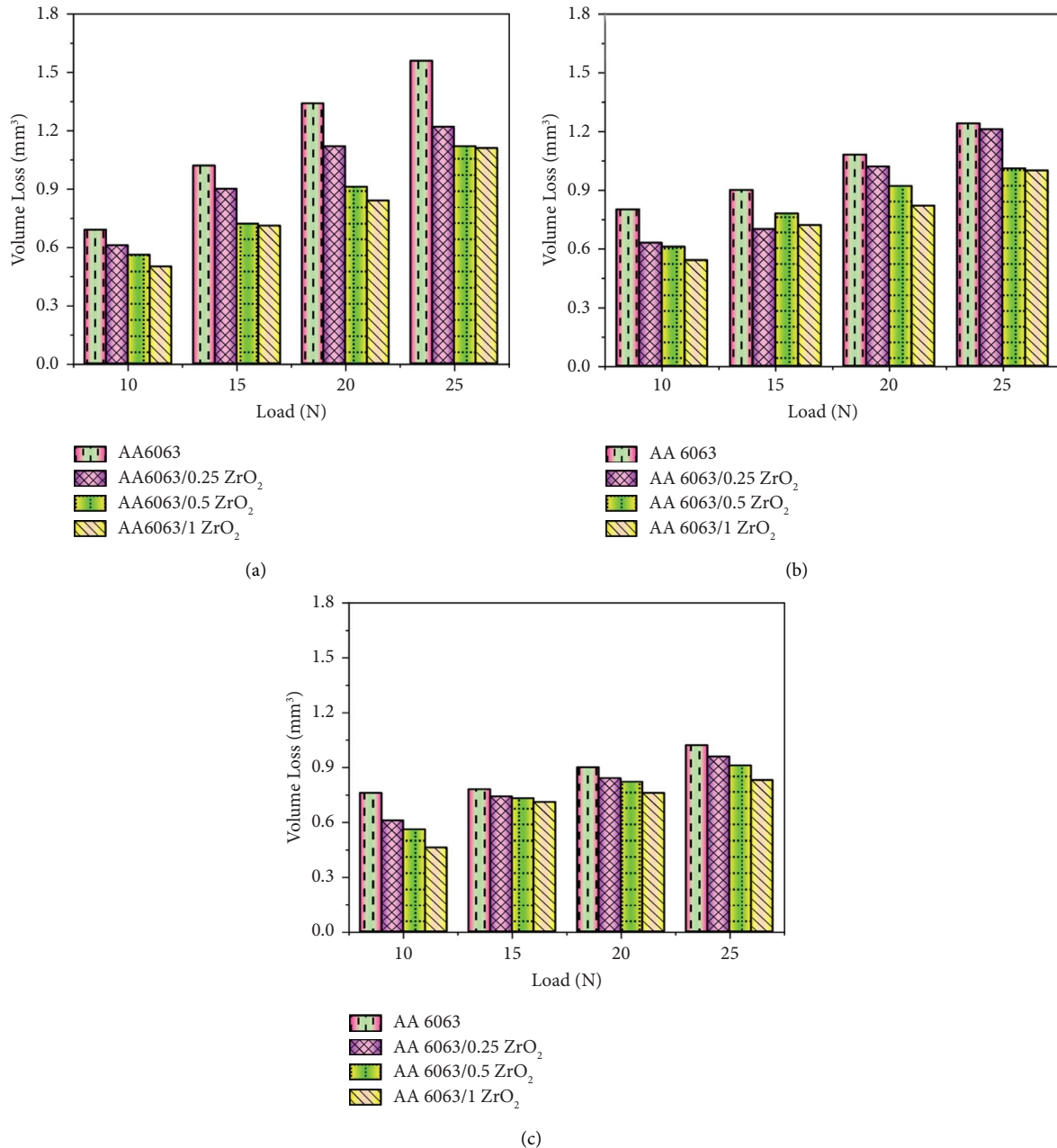


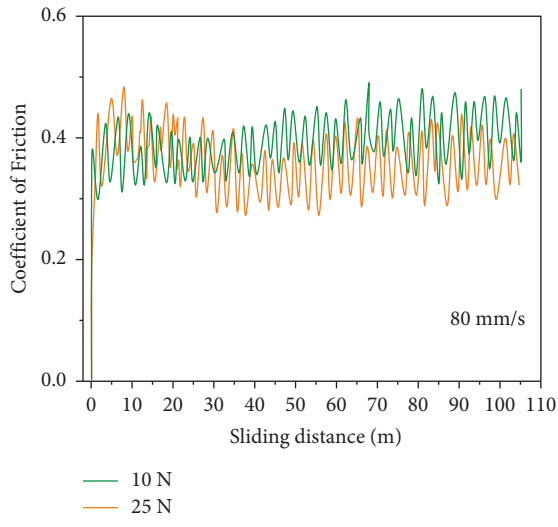
FIGURE 6: Variation of volume loss and load at variant sliding speeds: (a) 80, (b) 120, and (c) 150 mm/s.

higher hardness, which contributes to the material's exceptional wear resistance [41]. Results from this study on wear are consistent with Archard's law. There was a claim that more rigid materials have better tribological performance. Researchers have shown that incorporating nano-reinforcements into an Al matrix composite improves the wear resistance of the material.

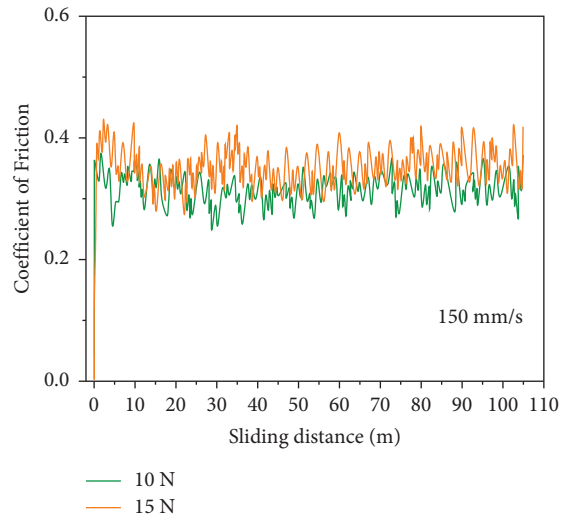
Graphs of the coefficients of friction (COF) under wear conditions (80 mm/s and 150 mm/s) are presented in Figures 7(a)–7(h). In particular, it was found that the mean COF of AA6063, AA6063/0.25 ZrO₂, AA6063/0.5 ZrO₂, and AA6063/1 ZrO₂ at loads of 10 and 25 N at sliding speeds of 80 mm/s was 0.363–0.391, 0.307–0.316, 0.245–0.267, and 0.214–0.224, respectively. With a sliding speed of 150 mm/s

and weights of 10 and 25 N, the mean COF of AA6063, AA6063/0.25 ZrO₂, AA6063/0.5 ZrO₂, and AA6063/1 ZrO₂ was calculated to be 0.335–0.367, 0.292–0.317, 0.231–0.253, and 0.213–0.226, respectively. The correlation between COF values and volume reduction was negative (Figures 5 and 6). Growing the strengthening in a structure improves its load-bearing volume and reduces the stress on the Al matrix. Shearing the reinforcement particles requires more energy. Hence, the composite surface has a lower friction coefficient [42].

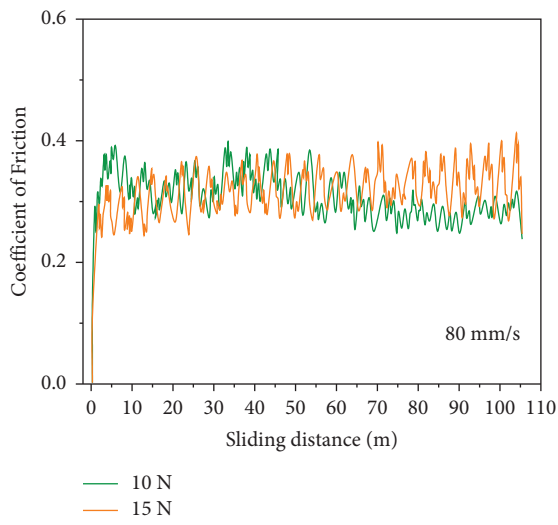
Particles on the worn surface further reduce friction by delaying strain hardening and plastic deformation [43]. Multiple studies have found that when reinforcement content increases, COF levels fall.



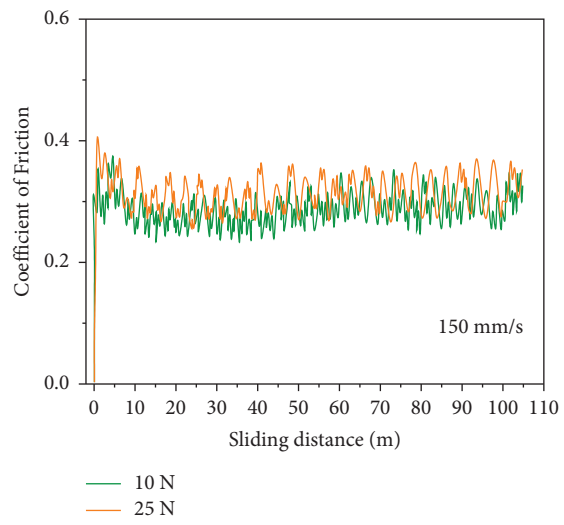
(a)



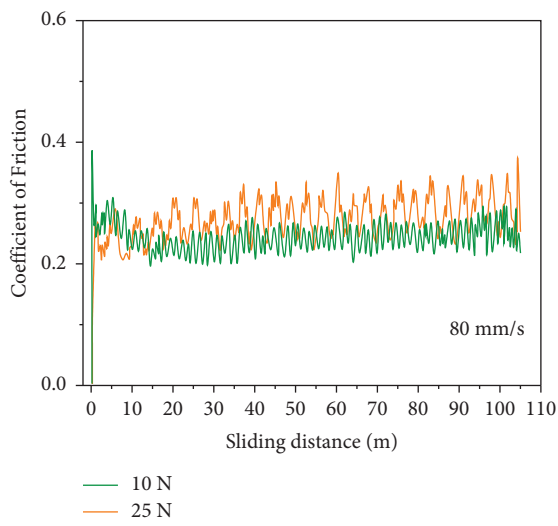
(b)



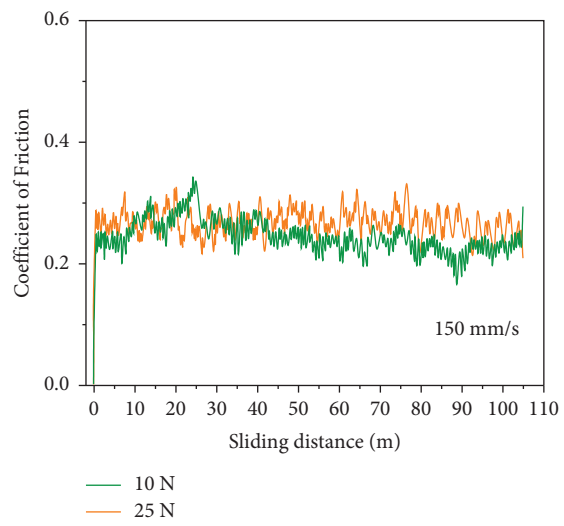
(c)



(d)



(e)



(f)

FIGURE 7: Continued.

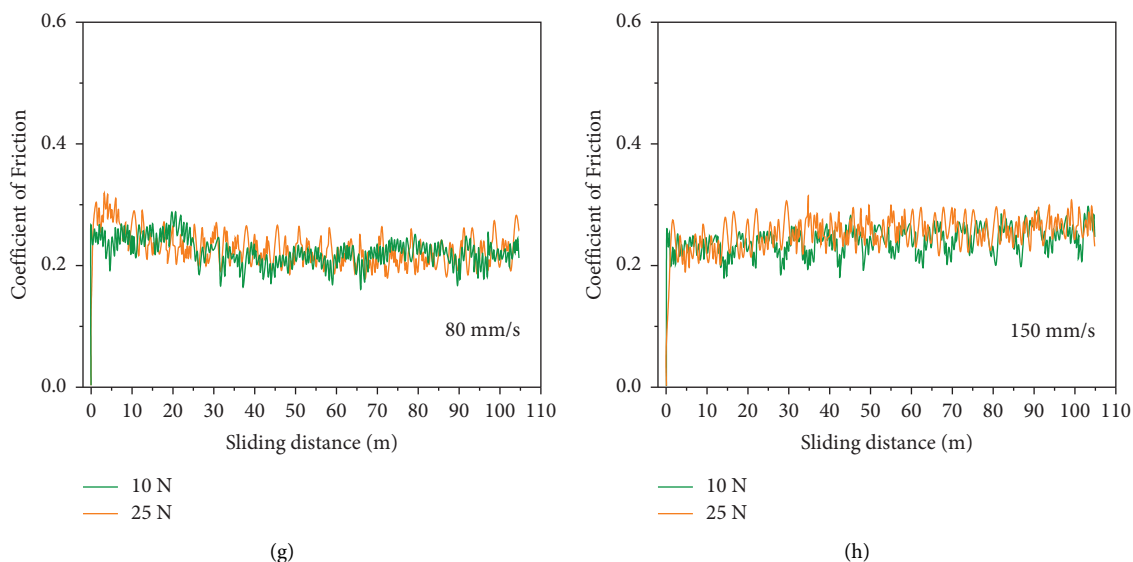


FIGURE 7: Evaluation of the coefficient of friction (a)-(b) AA6063, (c)-(d) AA6063/0.25 ZrO₂, (e)-(f) AA6063/0.5 ZrO₂, and (g)-(h) AA6063/1 ZrO₂.

Figure 7 shows that the COF increases with load, independent of material type, or sliding velocity. More plastic deformation occurred with a higher load, leading to a higher COF [44]. High loads cause plastic deformation and wear damage, as evidenced in the worn surface studies. Sliding faster results in a drop in the samples' COF levels, as observed in this research. According to the study, the COF drops as the wear rate rises because the oxides generated on the surface are constantly delaminating. Increased wear surface separation and larger delamination result from high speeds and contribute to a lower COF. The friction coefficient decreases due to oxygen entering metallic surfaces and forming an oxide coating on the surface.

3.3. Analysis of Worn Surface. Scanning electron microscope images of wear on the samples, taken at 80 mm/s, are shown in Figure 8(a). Even under a light 10 N load, there was evidence of deep grooves and worn detritus (Figure 8(b)). Wear caused by abrasion can be identified by grooves running perpendicular to the direction of sliding. Researchers have found that AA6063 alloy and its composites are susceptible to abrasion at low stresses [45]. When the load is increased, AA6063 alloy shows a significant delaminated region and some cracks. A large load causes shear deformation, which results in breaks during delamination wear. Under high load (25 N), the primary wear mechanism for AA6063/ZrO₂ hybrid composites was observed to be delamination and oxidation. Some grooves may be seen on the AA6063/0.25 ZrO₂ composite's worn surface.

At greater stress, the cracks and wear debris become apparent. Under a load of 10 N, the AA6063/0.5 ZrO₂ and AA6063/1 ZrO₂ surfaces show signs of wear in the form of scratches. As the load rises from 10 N to 25 N, craters and cracks appear on the AA6063/0.5 ZrO₂ and AA6063/1 ZrO₂ wear surfaces. Delamination wear leads to the creation of

craters. In the images of the worn surfaces of the samples, the transition from depth grooves to scrapes indicates that the character has experienced reduced wear damage as the ZrO₂ content increases during the sliding test at 80 mm/s and a force of 10 N. A 25 N load caused a vast section of the composite material to delaminate, creating a crater. This confirms the findings of the volume loss graph, which showed that AA6063/1 ZrO₂ showed the least amount of wear damage out of all the samples.

Figure 9 displays the EDS analyses of AA6063/0.25 ZrO₂ at 25 N and a sliding speed of 80 mm/s. As seen in an EDS study, both the first and second zones are rich in Al and O. This is because, at extreme friction (25 N), Al₂O₃ is formed. Because of this, authors might say that oxidized patches cover worn surfaces.

Figure 10 displays the outcomes of an EDS analysis conducted on the samples at a sliding speed of 150 mm/s. Several studies using the EDS analysis confirmed the existence of elevated O on worn surfaces for Al matrix composites. The energy dispersive spectroscopy analysis reveals exceptionally high concentrations of Al and Zr in the structure, indicating that these areas interact with compounds containing Al and Zr.

Moreover, the research revealed an amount of Zr within the specimen. After the wear test, the ZrO₂ nanoparticles were still present in the structure, proving their durability. Analysis by EDS revealed a high percentage (68.42%) of aluminum. Increases in sliding speed and ZrO₂ concentration are readily seen to reduce the material area moved into the counter-face ball. This is because the steel counter-face makes less contact with the Al matrix due to the presence of reinforcing particles (ZrO₂). It has been established through chemical analysis that the second section contains a high concentration of steel counter-face material, as evidenced by the presence of iron (55.7%), chromium (10.5%), and carbon (5.3%).

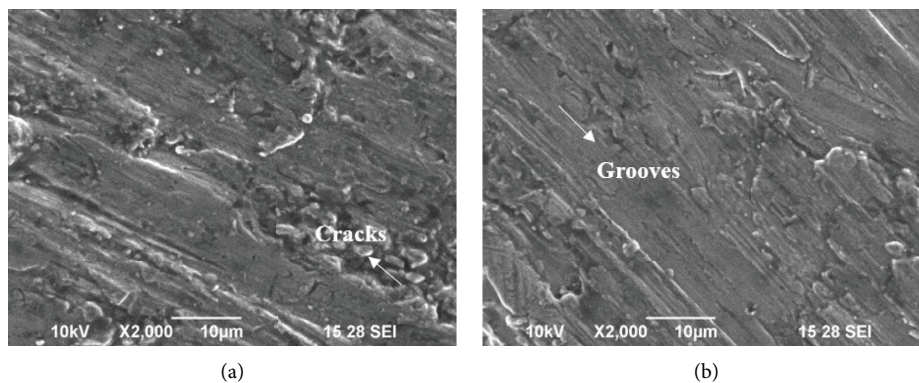


FIGURE 8: (a) AA6063 alloy and (b) AA6063/0.25 ZrO₂ for 10 N and worn surface of the specimen at 80 mm/s sliding speed.

4. The Methods of Machine Learning Models

Many supervised machine learning regression models have been developed to create a mapping function between the input characteristics (sliding speed, ZrO₂ content, and load) and the desired output feature (accuracy).

Before being fed into ML algorithms, data from actual experiments must be cleaned, sorted, and prepared. The information is then divided randomly into two groups: training data (75%) and validation data (25%). All three ML models are set up and educated on data sets. At the end of the training process, the stability of each ML model is evaluated using cross-validation. When assessing the efficiency of the training phase, the authors used 3-folds cross-validation, which involved splitting the training data into five sets and analyzing each group separately.

However, experimentation is necessary for determining the optimal settings for the machine learning model. The grid search method is utilized, with multiple variations of each model. The models were cross-validated against one another, and the optimal settings were identified using the training set. Therefore, the top estimators were applied to validation data, and the outcomes are shown here. The data must be cleaned and normalized for the ML model to have a high degree of accuracy. The data have been preprocessed using a standard scaling method for this application. To improve the ability to forecast the ML models, preprocessing normalizes all input and output features to the same scale.

4.1. ML Models. The support vector regressor (SVR), random forest (RF), and decision tree (DT) models, three of the most widespread and effective models in recent literature [46], have been chosen for a head-to-head performance comparison on the current dataset. Volume loss is a constant real value, and a regression can be used to predict its value. Python was used for all code implementations, and all the source code is available on the GitHub platform¹. The machine learning was accomplished with the help of the sci-kit learn libraries, and the visualization was performed using the seaborn libraries. This section briefly describes the theoretical foundations upon which algorithms are built. Readers interested in further exploring the topic of algorithms are directed to recent literature surveys of individual algorithms, which cover topics such as the algorithm's mathematical foundations and current uses.

4.1.1. Support Vector Regressor (SVR). For regression, SVR is a particular case of the original support vector machine. In support vector regressor, high-order hyperplanes are set up to establish a correlation between the input and the intended output measurement within predetermined limits. These hyperplanes are built using kernel functions, like radial basis and linear functions, to reduce the generalized error bound to a minimum. The regularization parameter and gamma are two primary parameters influencing the model's accuracy while constructing the hyperplanes. While SVR models can function with a small dataset, research in machine learning and tribology suggests that accuracy can be improved by providing high-dimensional data.

4.1.2. Decision Tree (DT). The DT technique constructs a tree-like structure with nodes and leaves to make predictions about the output data based on learning choice rules from the input dataset. The nodes make binary judgments dependent on the values of the input features, while the leaf displays a numerical goal. Splitting nodes can be done with the aid of mean squared error (MSE) and mean absolute error (MAE) functions. Even though increasing the tree's depth adds complexity to the model, doing so runs the risk of overfitting, wherein the model performs well on the training data because it has memorized the input but poorly on the testing data.

4.1.3. Random Forest (RF). The supervised machine learning model random forest is still another option. Classification problems shine the brightest although it also excels in regression. The random forest algorithm is called the ensemble technique that uses decision trees that have been randomly generated. It uses random data sampling from the training set to train various decision trees. The parameter n estimators, which represent the total number of trees in the forest, control how many trees will be created through the training phase. Inheritance from the DT model is used for the remaining model parameters.

4.2. Hyperparameter Tuning. The process of fine-tuning each parameter of ML model values has begun. Table 3 shows the various models and their respective setup parameters. For this reason, the factor subset combinations have been put up independently for each model due to their unique tuning parameters.

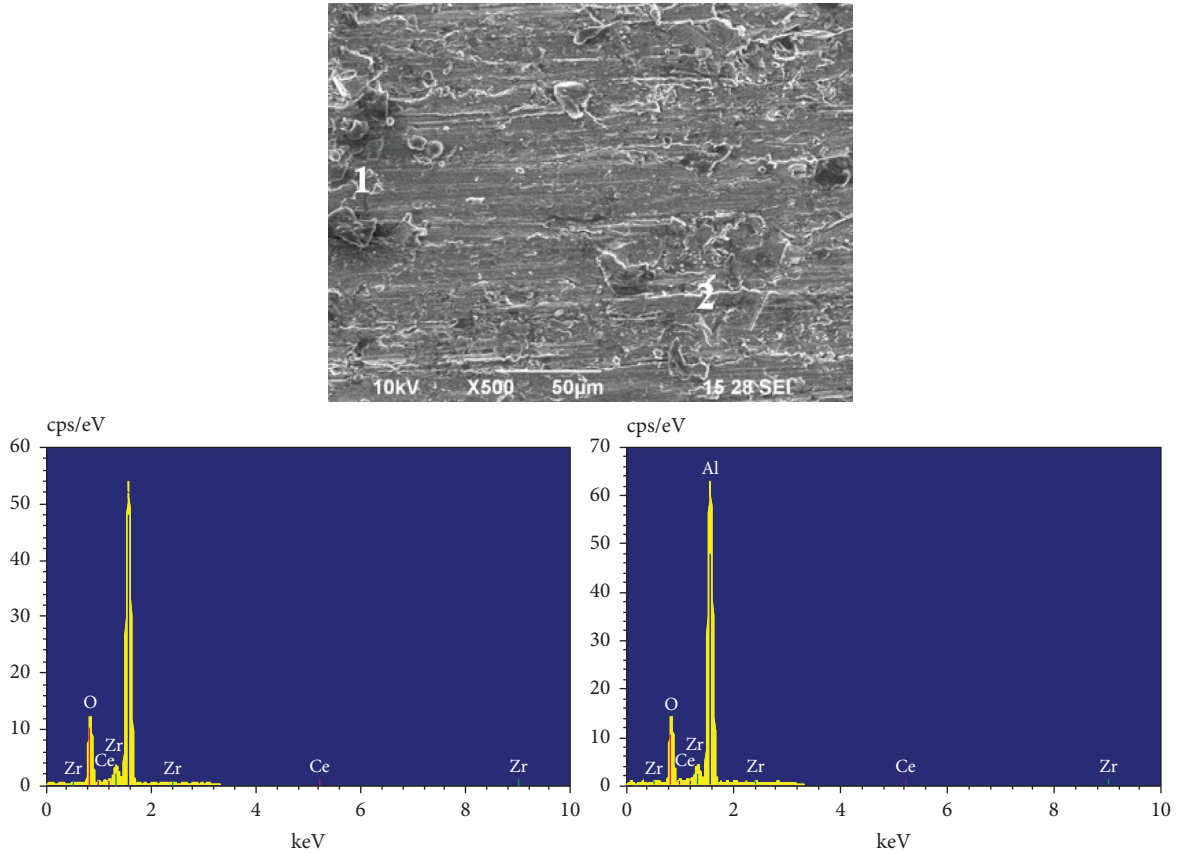


FIGURE 9: AA6063/0.25 ZrO₂ at 25 N for 80 mm/s analysis on EDS.

After finishing the hyperparameter tuning process, the optimal settings for each model may be identified. Results from experiments show that the optimal settings for SVR are as follows: regularization parameter $C=100$, rbf kernel, and coefficient $\gamma=0.001$. The optimal settings for RF include a maximum of two features per split (MF), one leaf node (MSL), and 100 decision trees (NE). Assuming a maximum depth of 8, the optimal splitting criterion for DT is absolute error and the minimum splitting level is set at 1.

A total of four measures (R^2 , RMSE, MSE, and MAE) were employed to evaluate the results of ML models. For scoring regression functions, authors utilize a statistic called R^2 , which is determined by the following formula:

$$R^2 = \frac{\sum_{i=1}^n (y_i - \hat{y}_i)^2}{\sum_{i=1}^n (y_i - \bar{y})^2}, \quad (2)$$

where n is the no. of tests, y_i is the real measuring output value, \hat{y}_i is the predicting output value, and \bar{y} is the mean value of y_i .

$$\text{RMSE} = \sqrt{\frac{\sum_{i=1}^n (y_i - \hat{y}_i)^2}{n}}. \quad (3)$$

Mean squared error (MSE) is the average squared deviation from the projected values.

$$\text{MSE} = \frac{\sum_{i=1}^n (y_i - \hat{y}_i)^2}{n}. \quad (4)$$

Mean absolute error (MAE) is the difference between the actual and expected values.

$$\text{MAE} = \frac{\sum_{i=1}^n |y_i - \hat{y}_i|}{n}. \quad (5)$$

The R^2 value of the model will be 1, and the others will be 0 if it is a perfect match for the data, as is evident from equation (2). R^2 provides more insight into the data's variability than the other three measures. Due to their monotonically connected representation of the squared errors among observed and predicted output values, RMSE and MSE are of interest. More resilient to outlier data, MAE also displays the mean value of the absolute error among the actual and predicted output values.

Models with optimal settings had the best R^2 , RMSE, MSE, and MAE values, shown in Table 4. Cross-validated training has allowed us to give mean and standard deviation. Table 4 indicates that DT is the most precise and reliable model, with a mean R^2 of 0.8580 and a standard deviation of 0.0220. Results on the test dataset showed that RF was competitive with DT.

The regression, root mean squared error, mean squared error, and mean absolute error for each algorithm volume loss validations are shown in Table 5. It has been claimed that

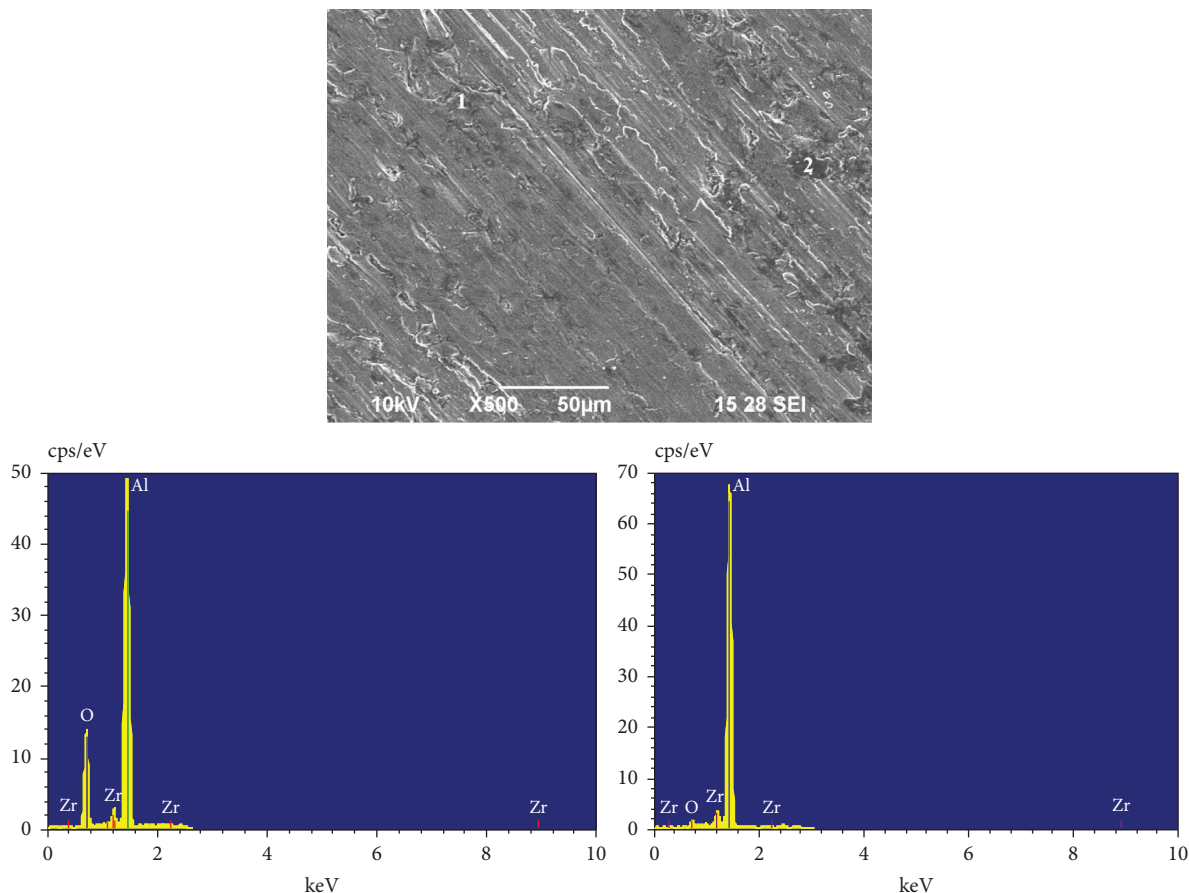
FIGURE 10: EDS specimen at 150 mm/s and AA6063/0.5 ZrO₂ (10 N).

TABLE 3: Models with a certain class of hypertuned parameters.

ML algorithms	Factors
RF	MF = {3, 4}, MSL = {4, 5, 6}, NE = {15, 25, 55, 100}
DT	S = {MSE, MAE}, MD = {1, 5, 7, 10}, MSL = {4, 5, 6}, MWFL = {0.1, 0.2, 0.5}
SVR	kernel = {rbf, linear}, gamma = {1e-4, 1e-5}, C = {1, 10, 100}

TABLE 4: Relative results of machine learning algorithms on testing data.

Metrics	Regression		Root mean squared error		Mean squared error		Mean absolute error	
	Mean	STD	Mean	STD	Mean	STD	Mean	STD
Machine learning algorithm								
Support vector regression	0.8186	0.0949	0.3774	0.1908	0.1788	0.1873	0.3055	0.1766
Random forest	0.8504	0.0599	0.3523	0.1502	0.1467	0.1381	0.2896	0.1126
Decision tree	0.8587	0.0226	0.3481	0.1114	0.1337	0.0917	0.2696	0.0924

values of R^2 for a model between 0.7 and 0.9 are acceptable. A model is deemed high quality if its R^2 value is more than 0.9. The R^2 value on the validation dataset ranged from 0.8078 to 0.9973 (Table 5). Tree-based ML models (RF and DT) outperformed higher-order models (SVR), which is an exciting finding. Therefore, the overfitting problem associated with limited data and the inability to generalize could be

a contributing factor. The fundamental disadvantage of tree-based approaches is that they need to be recreated and recalculated whenever new data is introduced to the current model because this impacts all prior iterations.

Figure 11 displays the predicted and observed volume decrease from each regressor. Volume loss was successfully expected by both RF(b) and DT(c). However, SVR (a) fared

TABLE 5: Relative results on machine learning algorithm on validating data.

Machine learning algorithms	Regression	Root mean squared error	Mean squared error	Mean absolute error
Support vector regression	0.8084	0.3922	0.1539	0.2578
Random forest	0.9784	0.1326	0.0183	0.0937
Decision tree	0.9926	0.0814	0.0071	0.0214

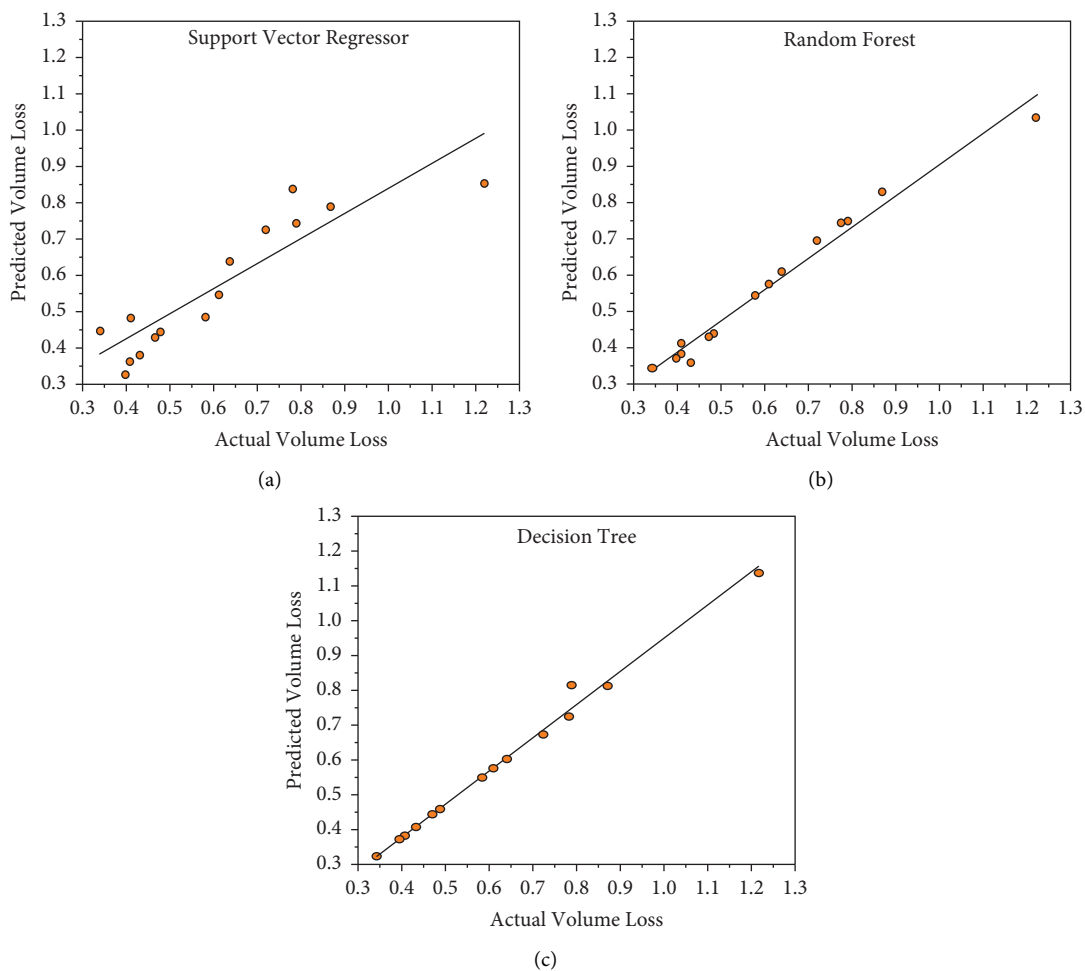


FIGURE 11: Evaluation of the actual volume loss and predicted volume loss by the machine learning algorithm.

poorly on the validation data set. SVR has a more significant margin of error compared to RF and DT.

As shown in Figure 12, the load, ZrO_2 content, and sliding speed are three of the most important input variables used by various ML models to estimate volume loss. Each variable affects the predicted volume loss, as shown in

Figure 12. The load was the primary factor in determining the outcome. According to various reports in the research literature, the load is the most critical factor when using machine learning to estimate wear rate. In contrast, the percentage of ZrO_2 and the sliding velocity were determined to be other crucial factors.

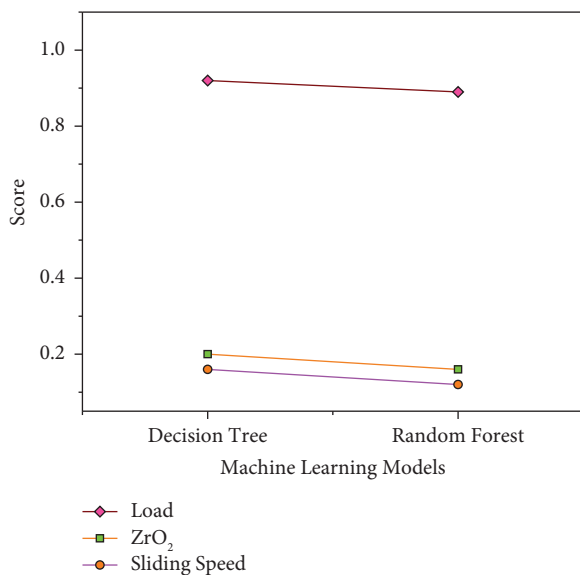


FIGURE 12: The significance of features in predicting volume loss.

5. Conclusions

In this research, the wear behavior and wear mechanism of a specimen made from an AA6063 matrix composite strengthened by ZrO₂ (0.25, 0.5, and 1 wt %) nanocomposites were examined after successful hot pressing. Wear resistance was predicted using three distinct machine learning methods. Here, the following are the most important findings:

- (i) By adding more ZrO₂, the resulting specimens were found to have a somewhat lower relative density. For the highest porosity (1.44%), the AA6063/1 ZrO₂ composite was used. A 1 wt% ZrO₂ component enhanced the hardness of the AA6063 alloy from a measured 66.1 to a measured 74.9.
- (ii) A study of the composite materials' microstructure reveals that the ZrO₂ nanoparticles aggregate into larger particles. X-ray diffraction testing confirms the existence of the Al, Al-Zr, and ZrO₂ phases.
- (iii) With the same load and sliding speeds, an increase in ZrO₂ content reduced volume loss.
- (iv) Abrasion was found to be a wear mechanism at 10 N, while abrasion and delamination were present at 25 N. Wear graphs showed that surfaces with higher ZrO₂ content showed reduced wear and damage.
- (v) Three machine learning algorithms were evaluated for their predictive abilities on a substantial experimental dataset.
- (vi) On this data set, tree-based decision algorithms performed the best. The accuracy of the decision tree algorithm's predictions for the test and validation measurements was 86% and 99.7%, respectively.
- (vii) Three ML techniques were used to state the relative weights of the input features explicitly. It has been

found that the load parameter has the most significant impact on the prediction of volume loss measurement.

Data Availability

The data used to support the findings of the study are included in the paper.

Ethical Approval

All procedures performed in this study involving human participants were by the ethical standards of the institutional and/or national research committee and its later amendments or comparable ethical standards.

Conflicts of Interest

The authors declare no that there are no conflicts of interest.

References

- [1] J. Arockia Dhanraj, B. Lingampalli, M. Prabhakar, A. Sivakumar, B. Krishnamurthy, and K. C. Ramanathan, "A credal decision tree classifier approach for surface condition monitoring of friction stir weldment through vibration patterns," *Materials Today Proceedings*, vol. 46, pp. 1127–1133, 2021.
- [2] U. Ali, W. Muhammad, A. Brahme, O. Skiba, and K. Inal, "Application of artificial neural networks in micromechanics for polycrystalline metals," *International Journal of Plasticity*, vol. 120, pp. 205–219, 2019.
- [3] Z. Zaidi, N. Maiti, M. I. Ali et al., "Fabrication, characteristics, and therapeutic applications of carbon-based nanodots," *Journal of Nanomaterials*, vol. 2022, Article ID 8031495, 12 pages, 2022.
- [4] I. Guagliardi, A. M. Astel, and D. Cicchella, "Exploring soil pollution patterns using self-organizing maps," *Toxics*, vol. 10, no. 8, p. 416, 2022.
- [5] T. A. Amibo, S. M. Beyan, M. Mustefa, V. P. Sundramurthy, and A. B. Bayu, "Development of nanocomposite based antimicrobial cotton fabrics impregnated by nano SiO₂ loaded AgNPs derived from eragrostis teff straw," *Materials Research Innovations*, vol. 26, no. 7, pp. 405–414, 2021.
- [6] A. Vasylenko, J. Gamon, B. B. Duff et al., "Element selection for crystalline inorganic solid discovery guided by unsupervised machine learning of experimentally explored chemistry," *Nature Communications*, vol. 12, no. 1, p. 5561, 2021.
- [7] Y. Wu and D. L. Irving, "Prediction of chemical ordering in refractory high-entropy superalloys," *Applied Physics Letters*, vol. 119, no. 11, Article ID 111901, 2021.
- [8] E. Varol Altay, E. Gurgenc, O. Altay, and A. Dikici, "Hybrid artificial neural network based on a metaheuristic optimization algorithm for the prediction of reservoir temperature using hydrogeochemical data of different geothermal areas in Anatolia (Turkey)," *Geothermics*, vol. 104, Article ID 102476, 2022.
- [9] K. Parkavi and P. Vivekanandan, "A novel cluster based energy efficient protocol for wireless networks," in *Proceedings of the IEEE-International Conference On Advances In Engineering, Science And Management (ICAESM-2012)*, pp. 645–650, Nagapattinam, India, March 2012.

- [10] P. Singh, D. Saucedo, and R. Arroyave, "High temperature oxidation behavior of disordered (Ti_{0.5}Zr_{0.5})₂AlC MAX phase via a Machine Learning-Augmented DFT approach," *Materials Letters X*, vol. 10, Article ID 100062, 2021.
- [11] A. Mariappan, "The application of energetic materials genome approach for development of the solid propellants through the space debris recycling at the space platform," in *Proceedings of the AIAA Propulsion and Energy 2020 Forum*, pp. 1–18, August 2020.
- [12] N. Sizochenko, M. Syzochenko, N. Fjodorova, B. Rasulev, and J. Leszczynski, "Evaluating genotoxicity of metal oxide nanoparticles: application of advanced supervised and unsupervised machine learning techniques," *Ecotoxicology and Environmental Safety*, vol. 185, Article ID 109733, 2019.
- [13] L. Shanmugam, K. Gunasekaran, A. Natarajan, and V. Kaliaperumal, "Quantitative growth analysis of pulp necrotic tooth (post op) using modified region growing active contour model," *IET Image Processing*, vol. 11, no. 11, pp. 1015–1019, 2017.
- [14] N. Venkatachalam, L. Shanmugam, G. C. Heltin, G. Govindarajan, and P. Sasipriya, "Enhanced segmentation of inflamed ROI to improve the accuracy of identifying benign and malignant cases in breast thermogram," *Journal of Oncology*, vol. 2021, Article ID 5566853, 17 pages, 2021.
- [15] R. Reena Roy and G. S. Anandha Mala, "Early detection of pancreatic cancer using jaundiced eye images," *Computer Systems Science and Engineering*, vol. 41, no. 2, pp. 677–688, 2022.
- [16] A. Jaiswal and Y. Zhang, "Robustness of dynamical cluster analysis in a glass-forming metallic liquid using an unsupervised machine learning algorithm," *MRS Advances*, vol. 1, no. 26, pp. 1929–1934, 2016.
- [17] C. Li, S. C. Yang, Q. S. Guo et al., "Determining the geographical origin of the medicinal plant *Marsdenia tenacissima* with multi-element analysis and data mining techniques," *Chemometrics and Intelligent Laboratory Systems*, vol. 136, pp. 115–120, 2014.
- [18] S. Kar, K. Pathakoti, P. B. Tchounwou, D. Leszczynska, and J. Leszczynski, "Evaluating the cytotoxicity of a large pool of metal oxide nanoparticles to *Escherichia coli*: mechanistic understanding through in Vitro and in Silico studies," *Chemosphere*, vol. 264, Article ID 128428, 2021.
- [19] T. Gurgenc, O. Altay, M. Ulas, and C. Ozel, "Extreme learning machine and support vector regression wear loss predictions for magnesium alloys coated using various spray coating methods," *Journal of Applied Physics*, vol. 127, no. 18, Article ID 185103, 2020.
- [20] O. A. Mohamed, S. H. Masood, and J. L. Bhowmik, "Experimental study of the wear performance of fused deposition modeling printed polycarbonate-acrylonitrile butadiene styrene parts using definitive screening design and machine learning-genetic algorithm," *Journal of Materials Engineering and Performance*, vol. 31, no. 4, pp. 2967–2977, 2022.
- [21] O. Altay, T. Gurgenc, M. Ulas, and C. Özel, "Prediction of wear loss quantities of ferro-alloy coating using different machine learning algorithms," *Friction*, vol. 8, no. 1, pp. 107–114, 2020.
- [22] A. M. Sadoun, I. Najjar, A. Fathy et al., "An enhanced Dendritic Neural Algorithm to predict the wear behavior of alumina coated silver reinforced copper nanocomposites," *Alexandria Engineering Journal*, vol. 65, pp. 809–823, 2023.
- [23] P. M. John, V. Periyasamy, and S. Arulnandhisivam, "Secure friend-based approach for ad-hoc routing using fuzzy random variables," *Int Inf Inst (Tokyo) Inf*, vol. 18, no. 2, p. 689, 2015.
- [24] V. Algur, P. Hulipalled, V. Loksha, M. Nagaral, and V. Auradi, "Machine learning algorithms to predict wear behavior of modified ZA-27 alloy under varying operating parameters," *Journal of Bio- and Tribo-Corrosion*, vol. 8, no. 1, p. 7, 2022.
- [25] T. Gurgenc and O. Altay, "Surface roughness prediction of wire electric discharge machining (WEDM)-machined AZ91D magnesium alloy using multilayer perceptron, ensemble neural network, and evolving product-unit neural network," *Materials Testing*, vol. 64, no. 3, pp. 350–362, 2022.
- [26] J. Singh and S. Singh, "Neural network supported study on erosive wear performance analysis of Y₂O₃/WC-10Co₄Cr HVOF coating," *Journal of King Saud University - Engineering Sciences*, vol. 35, 2022.
- [27] I. S. N. V. R. Prasanth, P. Jeevanandam, P. Selvaraju et al., "Study of friction and wear behavior of graphene-reinforced AA7075 nanocomposites by machine learning," *Journal of Nanomaterials*, vol. 2023, Article ID 5723730, 15 pages, 2023.
- [28] Y. Zhang, K. Mao, S. Leigh, A. Shah, Z. Chao, and G. Ma, "A parametric study of 3D printed polymer gears," *International Journal of Advanced Manufacturing Technology*, vol. 107, no. 11–12, pp. 4481–4492, 2020.
- [29] M. G. Shirangi, E. Furlong, and K. S. Sims, "Digital twins for well planning and bit dull grade prediction," 2020, <https://www.scopus.com/inward/record.uri?eid=2-s2.0-85086241879&partnerID=40&md5=5f6f37353a421844eaa263245179a32b>.
- [30] S. Mayakannan, R. Rathinam, R. Saminathan et al., "Analysis of spectroscopic, morphological characterization and interaction of dye molecules for the surface modification of TiB₂Nanoparticles," *Journal of Nanomaterials*, vol. 2022, Article ID 1033216, 9 pages, 2022.
- [31] M. Ulas, O. Aydur, T. Gurgenc, and C. Ozel, "Surface roughness prediction of machined aluminum alloy with wire electrical discharge machining by different machine learning algorithms," *Journal of Materials Research and Technology*, vol. 9, no. 6, pp. 12512–12524, 2020.
- [32] G. Sathiaraj, R. Mani, M. Muthuraj, and S. Mayakannan, "The mechanical behavior of Nano sized Al₂O₃ -reinforced Al-Si7-Mg alloy fabricated by powder metallurgy and forging," *ARPJN Journal of Engineering and Applied Sciences*, vol. 11, no. 9, pp. 6056–6061, 2016.
- [33] P. Esch and F. Werner-Jäger, "Anwendung eines künstlichen Neuronalen Netzes zur Verschleißbestimmung von Zerspanwerkzeugen: KI-gerechte Datenaufbereitung zum Anlernen eines Neuronalen Netzwerks," *At-Automatisierungstechnik*, vol. 70, no. 7, pp. 635–645, 2022.
- [34] F. Aydin, "The investigation of the effect of particle size on wear performance of AA7075/Al₂O₃ composites using statistical analysis and different machine learning methods," *Advanced Powder Technology*, vol. 32, no. 2, pp. 445–463, 2021.
- [35] S. Thangaraj, G. M. Pradeep, M. S. Heaven Dani, S. Mayakannan, and A. Benham, "Experimental investigations on tensile and compressive properties of nano alumina and arecanut shell powder reinforced polypropylene hybrid composites," *Materials Today: Proceedings*, vol. 68, pp. 2243–2248, 2022.
- [36] F. Aydin and R. Durgut, "Estimation of wear performance of AZ91 alloy under dry sliding conditions using machine learning methods," *Transactions of Nonferrous Metals Society of China*, vol. 31, no. 1, pp. 125–137, 2021.
- [37] A. P. Sekhar and D. Das, "Influence of artificial aging on mechanical properties and high stress abrasive wear

- behaviour of Al–Mg–Si alloy,” *Metals and Materials International*, vol. 27, no. 2, pp. 337–351, 2021.
- [38] B. Stalin, P. Ramesh Kumar, M. Ravichandran, M. Siva Kumar, and M. Meignanamoorthy, “Optimization of wear parameters using Taguchi grey relational analysis and ANN-TLBO algorithm for silicon nitride filled AA6063 matrix composites,” *Materials Research Express*, vol. 6, no. 10, Article ID 106590, 2019.
- [39] G. N. K. G Naveen Kumar et al, V. Mahidhar Reddy, M. Sunil Kumar, K. Hemachandra Reddy, and Y. V. Mohana Reddy, “Slurry erosive wear behavior of AA 6063/TiC particles in situ composites,” *International Journal of Mechanical and Production Engineering Research and Development*, vol. 7, no. 3, pp. 223–232, 2017.
- [40] S. Ilangovan, A. Shanmugasundaram, and S. Arul, “Influence of specimen temperature on wear characteristics of aa6063 aluminium alloy,” *Journal of Surface Science and Technology*, vol. 32, no. 3–4, pp. 93–98, 2017.
- [41] P. A. Sylajakumari, R. Ramakrishnasamy, and G. Palaniappan, “Taguchi grey relational analysis for multi-response optimization of wear in co-continuous composite,” *Materials*, vol. 11, 9 pages, 2018.
- [42] N. Kaushik and S. Singhal, “Examination of wear properties in dry-sliding states of SIC strengthened al-alloy metal matrix composites by using taguchi optimization approach,” *International Journal of Applied Engineering Research*, vol. 12, no. 20, pp. 9708–9716, 2017.
- [43] P. Kiss, D. Fonyo, and T. Horvath, “BlaBoO: a lightweight black box optimizer framework,” in *Proceedings of the DISA 2018 - IEEE World Symposium on Digital Intelligence for Systems and Machines*, pp. 213–218, Slovakia, August 2018.
- [44] T. M. Deist, F. J. W. M. Dankers, G. Valdes et al., “Machine learning algorithms for outcome prediction in (chemo)radiotherapy: an empirical comparison of classifiers,” *Medical Physics*, vol. 45, no. 7, pp. 3449–3459, 2018.
- [45] J. Gao, D. Nuyttens, P. Lootens, Y. He, and J. G. Pieters, “Recognising weeds in a maize crop using a random forest machine-learning algorithm and near-infrared snapshot mosaic hyperspectral imagery,” *Biosystems Engineering*, vol. 170, pp. 39–50, 2018.
- [46] W. Brendel, J. Rauber, and M. Bethge, “Decision-based adversarial attacks: reliable attacks against black-box machine learning models,” 2018, <https://www.scopus.com/inward/record.uri?eid=2-s2.0-85083954048&partnerID=40&md5=d2646cdf5c872ab2eaf5119b5338131f>.